

UNROLLING NONCONVEX GRAPH TOTAL VARIATION FOR IMAGE DENOISING

Songlin Wei*, Gene Cheung†, Fei Chen*, Ivan Selesnick#

†York University, Canada

*Fuzhou University, China

#New York University, USA

ABSTRACT

Conventional model-based image denoising optimizations employ convex regularization terms, such as total variation (TV) that convexifies the ℓ_0 -norm to promote sparse signal representation. Instead, we propose a new non-convex total variation term in a graph setting (NC-GTV), such that when combined with an ℓ_2 -norm fidelity term for denoising, leads to a convex objective with no extraneous local minima. We define NC-GTV using a new graph variant of the Huber function, interpretable as a Moreau envelope. The crux is the selection of a parameter a characterizing the graph Huber function that ensures overall objective convexity; we efficiently compute a via an adaptation of Gershgorin Circle Theorem (GCT). To minimize the convex objective, we design a linear-time algorithm based on Alternating Direction Method of Multipliers (ADMM) and unroll it into a lightweight feed-forward network for data-driven parameter learning. Experiments show that our method outperforms unrolled GTV and other representative image denoising schemes, while employing far fewer network parameters.

Index Terms— Image denoising, graph signal processing, convex optimization, algorithm unrolling

1. INTRODUCTION

Image denoising [1] is a well-studied basic restoration problem that remains important today; other image restoration tasks like deblurring [2] can be addressed using general frameworks like the *Plug-and-Play Alternating Direction Method of Multipliers* (PnP-ADMM) [3] that employ an image denoiser as a building block, and popular generative diffusion models can be implemented as cascades of image denoisers [4]. While *deep learning* (DL) based denoisers [5] are now prevalent and achieve state-of-the-art (SOTA) performance, they are inherent “black boxes” that are uninterpretable and employ a huge number of network parameters, and thus are not suitable for memory-constrained devices. In contrast, an alternative hybrid model-based / data-driven paradigm called *algorithm unrolling* [6] builds an

The work of G. Cheung was supported in part by the Natural Sciences and Engineering Research Council of Canada (NSERC) RGPIN-2025-06252. The work of F. Chen was supported in part by the National Natural Science Foundation of China (62471141).

interpretable neural net by implementing each iteration of a model-based iterative algorithm as a neural layer towards a feed-forward network amenable to parameter learning. We pursue this paradigm here for image denoising, but from a *graph signal processing* (GSP) perspective [7, 8].

Model-based image denoisers commonly formulate an optimization with a convex regularization term such as *total variation* (TV) [9]—convexification of the combinatorial ℓ_0 -norm to promote sparse signal restoration (*i.e.*, sparse discontinuities for an otherwise smooth signal). However, a large signal discontinuity $|x_{i+1} - x_i|$ at pixel i has much larger ℓ_1 -norm than ℓ_0 -norm, and thus minimizing TV tends to underestimate signal discontinuities, resulting in sub-optimal reconstructions of *piecewise constant* (PWC) signals.

To improve upon TV, for one-dimensional signals [10] pursued a *convex non-convex* (CNC) strategy [11, 12]: combine a non-convex regularization term (called the *minimax-concave* (MC) function)—which reduces the underestimation of signal discontinuities—with a convex fidelity term, so that the overall objective remains convex, thereby mitigating the problem of extraneous local minima. [10] demonstrated better PWC signal recovery than TV for 1D signal denoising.

Inspired by [10], we propose *non-convex graph total variation* (NC-GTV)—extension of MC function to the graph domain—for image denoising. Specifically, we define NC-GTV using a new graph variant of the *Huber function* [13], which is interpretable as a Moreau envelope [14]. The crux is the selection of a MC parameter a characterizing the graph Huber function that ensures overall objective convexity; we efficiently compute a via a clever adaptation of *Gershgorin Circle Theorem* (GCT) [15]. To minimize the convex objective, we design a linear-time algorithm based on *Alternating Direction Method of Multipliers* (ADMM) [16] and unroll it into a lightweight feed-forward network for data-driven parameter learning. Experiments show that our method outperforms unrolled GTV and other representative model-based and deep-learning-based image denoising schemes [17, 5], while employing drastically fewer network parameters.

We summarize our contributions as follows:

1. We design a graph Huber function $S_a(\mathbf{x}', \mathbf{x})$ —extension of the scalar Huber function $s_a(x)$ to the graph domain—as a quadratic term using penalty graph Laplacian \mathbf{L}_a^p that is amenable to fast optimization. Like $s_a(x)$, we show $S_a(\mathbf{x}', \mathbf{x})$ is interpretable as a Moreau envelope.

2. Leveraging GCT, we efficiently compute the “tightest” parameter a characterizing the graph Huber function that guarantees PSDness of coefficient matrix $\mathbf{I} - \mu \mathbf{L}_a^p$, and hence convexity of the optimization objective.
3. We unroll an ADMM algorithm into a lightweight interpretable feed-forward network for data-driven parameter learning, with competitive denoising performance.

2. PRELIMINARIES

2.1. GSP Definitions

A positive undirected graph $\mathcal{G} = (\mathcal{V}, \mathcal{E}, \mathbf{W})$ is defined by a node set $\mathcal{V} = \{1, \dots, N\}$ and an edge set $\mathcal{E} = \{(i, j)\}$ with $M = |\mathcal{E}|$ edges, where edge $(i, j) \in \mathcal{E}$ has non-negative weight $w_{i,j} = W_{i,j}$, for *adjacency matrix* $\mathbf{W} \in \mathbb{R}^{N \times N}$. Undirected edges mean that $W_{i,j} = W_{j,i}$, and \mathbf{W} is symmetric. *Degree matrix* $\mathbf{D} \in \mathbb{R}^{N \times N}$ is a diagonal matrix with diagonal entries $D_{i,i} = \sum_j W_{i,j}$. The combinatorial *graph Laplacian matrix* $\mathbf{L} \in \mathbb{R}^{N \times N}$ [7] is defined as

$$\mathbf{L} \triangleq \mathbf{D} - \mathbf{W} = \text{diag}(\mathbf{W}\mathbf{1}) - \mathbf{W}, \quad (1)$$

where $\mathbf{1}$ is an all-one vector of appropriate length, and $\text{diag}(\mathbf{v})$ is the diagonal matrix containing vector \mathbf{v} as diagonal entries. \mathbf{L} is provably *positive semi-definite* (PSD) if all edge weights are non-negative, *i.e.*, $W_{i,j} \geq 0, \forall i, j$ [8].

Real and symmetric Laplacian \mathbf{L} can be eigen-decomposed to $\mathbf{L} = \mathbf{V}\Lambda\mathbf{V}^\top$, where \mathbf{V} contains eigenvectors of \mathbf{L} as columns, and $\Lambda = \text{diag}(\lambda_1, \dots, \lambda_N)$ is a diagonal matrix with ordered eigenvalues $0 = \lambda_1 \leq \lambda_2 \leq \dots \leq \lambda_N$ along its diagonal. The k -th eigen-pair $(\lambda_k, \mathbf{v}_k)$ is the k -th graph frequency and Fourier mode for \mathcal{G} , respectively. $\tilde{\mathbf{x}} = \mathbf{V}^\top \mathbf{x}$ is the *graph Fourier transform* (GFT) of signal \mathbf{x} [7], where $\tilde{x}_k = \mathbf{v}_k^\top \mathbf{x}$ is the k -th GFT coefficient for signal \mathbf{x} .

2.2. Graph Laplacian Regularizer

To regularize an ill-posed graph signal restoration problem like denoising [18] or quantization [19], *graph Laplacian regularizer* (GLR) is popular due to its convenient quadratic form that is amenable to fast optimization [18]. Given a positive graph \mathcal{G} specified by graph Laplacian \mathbf{L} , GLR for a signal $\mathbf{x} \in \mathbb{R}^N$ is defined as

$$\mathbf{x}^\top \mathbf{L} \mathbf{x} = \sum_{(i,j) \in \mathcal{E}} w_{i,j} (x_i - x_j)^2 = \sum_k \lambda_k \tilde{x}_k^2. \quad (2)$$

Thus, minimizing GLR means promoting a signal with connected sample pairs (x_i, x_j) that are similar. In the spectral domain, it means promoting a *low-pass* signal with energies \tilde{x}_k^2 ’s concentrated in low graph frequencies λ_k ’s.

2.3. Graph Total Variation

Another popular graph signal regularization term is *graph total variation* (GTV) [20, 21, 2]. Define first the *incidence matrix* $\mathbf{C} \in \mathbb{R}^{M \times N}$ as

$$C_{m,j} = \begin{cases} w_{i,j} & \text{if start node of } m\text{-th edge } (j, i) \text{ is } j \\ -w_{i,j} & \text{if end node of } m\text{-th edge } (i, j) \text{ is } j \\ 0 & \text{o.w.} \end{cases}. \quad (3)$$

Given an undirected graph \mathcal{G} , the start and end nodes of each edge (i, j) are arbitrary. We can now define GTV as

$$\|\mathbf{C}\mathbf{x}\|_1 = \sum_{(i,j) \in \mathcal{E}} w_{i,j} |x_i - x_j|. \quad (4)$$

(4) is essentially the ℓ_1 -norm variant of GLR (2).

3. PROBLEM FORMULATION

3.1. Defining Graph Huber Function

3.1.1. MC penalty and Huber Functions

From [10], the scalar *minimax-concave* (MC) penalty function $\phi_a(x) : \mathbb{R} \mapsto \mathbb{R}_+$ is defined as

$$\phi_a(x) = \begin{cases} |x| - \frac{a}{2}x^2 & \text{if } |x| \leq \frac{1}{a} \\ \frac{1}{2a} & \text{o.w.} \end{cases} \quad (5)$$

where $a > 0$ is a non-negative *MC parameter*. Note that for $a = 0$, $\phi_a(x) = |x|$, *i.e.*, the ℓ_1 -norm.

The MC penalty function can be written in terms of the *Huber function* [13] $s_a(x)$, *i.e.*, $\phi_a(x) = |x| - s_a(x)$, where $s_a(x)$ is defined as

$$s_a(x) = \begin{cases} \frac{a}{2}x^2 & \text{if } |x| \leq \frac{1}{a} \\ |x| - \frac{1}{2a} & \text{o.w.} \end{cases}. \quad (6)$$

The Huber function $s_a(x)$ can also be written in terms of the *Moreau envelope* [14] $f^M(x)$ defined as

$$f^M(\mathbf{x}) \triangleq \inf_{\mathbf{v} \in \mathbb{R}^N} \left\{ f(\mathbf{v}) + \frac{1}{2} \|\mathbf{x} - \mathbf{v}\|_2^2 \right\} \quad (7)$$

$$s_a(x) = \min_v \left\{ |v| + \frac{a}{2} (x - v)^2 \right\} = a \left(\frac{1}{a} |\cdot| \right)^M(x). \quad (8)$$

3.1.2. Graph Huber Function

We construct a graph variant of $s_a(x)$ for graph signal $\mathbf{x} \in \mathbb{R}^N$, called *graph Huber function*, given a positive undirected graph $\mathcal{G}(\mathcal{V}, \mathcal{E}, \mathbf{W})$. The idea is to mimic (6), where for each connected pair $(i, j) \in \mathcal{E}$, we construct an ℓ_2 -norm $w_{i,j}(x_i - x_j)^2$ scaled by $\frac{a}{2}$ if $|x_i - x_j| \leq \frac{1}{a}$, and an ℓ_1 -norm $w_{i,j}|x_i - x_j|$ minus constant $\frac{w_{i,j}}{2a}$ otherwise. We seek to express the sum of terms for all connected pairs (i, j) in a compact quadratic form $\mathbf{x}^\top \mathbf{L}_a^p \mathbf{x}$, for some graph Laplacian matrix \mathbf{L}_a^p (p means “penalty” here, while a parameterizes \mathbf{L}_a^p).

For each edge $(i, j) \in \mathcal{E}$, we first define a *signal-dependent* edge weight $w_{i,j}^p$ for a corresponding *penalty graph* \mathcal{G}^p as

$$w_{i,j}^p = \begin{cases} \frac{a}{2} w_{i,j} & \text{if } |x'_i - x'_j| \leq \frac{1}{a} \\ \frac{w_{i,j}}{\max(|x'_i - x'_j|, \epsilon)} & \text{if } |x'_i - x'_j| > \frac{1}{a} \\ 0 & \text{o.w.} \end{cases} \quad (9)$$

where x'_i is the most recent estimate of signal sample at node i , and $\epsilon > 0$ is a small positive parameter for numerical stability, similarly done in [2].

The set of edge weights $\{w_{i,j}^p\}$ thus specifies an adjacency matrix \mathbf{W}_a^p , and we can define a corresponding combinatorial graph Laplacian as $\mathbf{L}_a^p \triangleq \text{diag}(\mathbf{W}_a^p \mathbf{1}) - \mathbf{W}_a^p$. Thus, signal-dependent GLR $\mathbf{x}^\top \mathbf{L}_a^p(\mathbf{x}') \mathbf{x}$ is

$$\begin{aligned} & \approx \sum_{(i,j) \in \mathcal{E} \mid |x'_i - x'_j| \leq \frac{1}{a}} \frac{a}{2} w_{i,j} (x_i - x_j)^2 + \sum_{(i,j) \in \mathcal{E} \mid |x'_i - x'_j| > \frac{1}{a}} w_{i,j} |x_i - x_j| \\ & - \sum_{(i,j) \in \mathcal{E} \mid |x'_i - x'_j| > \frac{1}{a}} \frac{w_{i,j}}{2a} \end{aligned} \quad (10)$$

assuming $x'_i \approx x_i, \forall i$. We see that (10) is a graph variant of the Huber function (6): for each edge $(i, j) \in \mathcal{E}$ where $|x'_i - x'_j| \leq \frac{1}{a}$, GLR computes $\frac{a}{2} w_{i,j} (x_i - x_j)^2$, and for each edge $(i, j) \in \mathcal{E}$ where $|x'_i - x'_j| > \frac{1}{a}$, GLR computes

$$\begin{aligned} & \frac{w_{i,j}}{|x'_i - x'_j|} (x_i - x_j)^2 - \frac{w_{i,j}}{2a(x'_i - x'_j)^2} (x_i - x_j)^2 \\ & \approx w_{i,j} |x_i - x_j| - \frac{w_{i,j}}{2a}, \end{aligned}$$

assuming $|x'_i - x'_j| > \epsilon$. For $|x'_i - x'_j| < \epsilon$, the GLR term for edge (i, j) is near zero anyway.

We can now define a signal-dependent graph Huber function $S_a(\mathbf{x}', \mathbf{x})$ as

$$S_a(\mathbf{x}', \mathbf{x}) \triangleq \mathbf{x}^\top \mathbf{L}_a^p(\mathbf{x}') \mathbf{x}. \quad (11)$$

Note that the graph Huber function $S_a(\mathbf{x}', \mathbf{x})$ is continuous w.r.t. $|x_i - x_j|$; when $|x_i - x_j| = \frac{1}{a}$, contribution from edge (i, j) is $\frac{a}{2} w_{i,j} (x_i - x_j)^2 = \frac{w_{i,j}}{2a}$, and when $|x_i - x_j| = \frac{1}{a} + \gamma$, for $\gamma \rightarrow 0^+$, contribution is also $w_{i,j} |x_i - x_j| - \frac{w_{i,j}}{2a} = \frac{w_{i,j}}{2a}$.

Note also that like $s_a(x)$ in (7), $S_a(\mathbf{x}', \mathbf{x})$ can also be written as a Moreau Envelope:

$$S_a(\mathbf{x}', \mathbf{x}) = \min_{\mathbf{v} \in \mathbb{R}^M} \left\{ \|\mathbf{v}\|_1 + \frac{a}{2} \|\mathbf{C}\mathbf{x} - \mathbf{v}\|_2^2 \right\} = a \left(\frac{1}{a} \|\mathbf{1}\| \cdot \|\mathbf{1}\|^M (\mathbf{C}\mathbf{x}) \right). \quad (12)$$

3.2. Defining Objective

We now define our signal denoising objective as follows. The objective is a sum of the ℓ_2 -norm fidelity term, plus the graph variant of the MC penalty term (5)—GTV (4) minus the graph Huber function (11):

$$\min_{\mathbf{x}} \|\mathbf{y} - \mathbf{x}\|_2^2 + \mu \|\mathbf{C}\mathbf{x}\|_1 - \mu \mathbf{x}^\top \mathbf{L}_a^p(\mathbf{x}') \mathbf{x}, \quad (13)$$

where $\mu > 0$ is a regularizer weight parameter. We observe that (13) is a ℓ_1 -/ ℓ_2 -norm minimization problem. For the objective to be convex, we first rewrite it as

$$\mathbf{y}^\top \mathbf{y} - 2\mathbf{x}^\top \mathbf{y} + \mathbf{x}^\top (\mathbf{I} - \mu \mathbf{L}_a^p(\mathbf{x}')) \mathbf{x} + \mu \|\mathbf{C}\mathbf{x}\|_1$$

which is convex if $\mathbf{I} - \mu \mathbf{L}_a^p(\mathbf{x}')$ is PSD.

3.3. MC Parameter Selection

Edge weight $w_{i,j}^p$ is computed differently in (9) depending on $|x'_i - x'_j|$ relative to $\frac{1}{a}$. Specifically, when $|x'_i - x'_j| = \frac{1}{a}$, edge weight $w_{i,j}^p \leftarrow \frac{a}{2} w_{i,j}$ in both computations. When $|x'_i - x'_j| < \frac{1}{a}$, $w_{i,j}^p$ increases linearly with a , and when $|x'_i - x'_j| > \frac{1}{a}$, $w_{i,j}^p$ increases more slowly with $\frac{1}{a}$. Given that $w_{i,j}^p$ increases with a generally but at two different rates, we compute a largest parameter a^* while ensuring $\mathbf{I} - \mu \mathbf{L}_a^p(\mathbf{x}')$ is PSD, leveraging the *Gershgorin Circle Theorem* (GCT) [15], as follows.

Define $\mathbf{B} \triangleq \mathbf{I} - \mu \mathbf{L}_a^p(\mathbf{x}')$. By GCT, a lower bound λ_{\min}^- for the smallest eigenvalue λ_{\min} of \mathbf{B} is

$$\lambda_{\min}^-(\mathbf{B}) \triangleq \min_i B_{i,i} - \sum_{j \mid j \neq i} |B_{i,j}|, \quad (14)$$

where $c_i = B_{i,i}$ and $r_i = \sum_{j \neq i} |B_{i,j}|$ are the center and radius of the i -th Gershgorin disc of matrix \mathbf{B} , respectively. We select the largest a (to maximize the effectiveness of the MC penalty function) while ensuring \mathbf{B} is PSD, *i.e.*,

$$a^* = \arg \max_a a, \quad \text{s.t. } \lambda_{\min}^-(\mathbf{B}) \geq 0. \quad (15)$$

Given \mathbf{x}' , we sort $\frac{1}{|x'_i - x'_j|}$ for each $(i, j) \in \mathcal{E}$ into a list \mathcal{S} of increasing magnitude; these are the a values at which an edge weight $w_{i,j}^p$ switches from one computation to another via (9). We identify the largest value $a^l \in \mathcal{S}$ such that $\lambda_{\min}^-(\mathbf{B}) \geq 0$ via *binary search* [22]. Denote by a^u the next larger value in \mathcal{S} . We then compute the following three subset sums for each row i of \mathbf{B} :

$$\tilde{r}_i^{(1)} = \frac{1}{2} \sum_{j \mid (i,j) \in \mathcal{E}, |x'_i - x'_j| \leq \frac{1}{a^l}} w_{i,j} \quad (16)$$

$$\tilde{r}_i^{(2)} = \sum_{j \mid (i,j) \in \mathcal{E}, |x'_i - x'_j| > \frac{1}{a^l}} \frac{w_{i,j}}{\max(|x'_i - x'_j|, \epsilon)} \quad (17)$$

$$\tilde{r}_i^{(3)} = \frac{1}{2} \sum_{j \mid (i,j) \in \mathcal{E}, |x'_i - x'_j| > \frac{1}{a^l}} \frac{-w_{i,j}}{\max((x'_i - x'_j)^2, \epsilon)} \quad (18)$$

Note that the i -th disc radius of \mathbf{B} is $r_i = \mu(\tilde{r}_i^{(1)} + \tilde{r}_i^{(2)} + \tilde{r}_i^{(3)})/a$. To identify the largest a_i^* for this row, we set $c_i - r_i = 0$, where $c_i = B_{i,i} = 1 - \mu(\mathbf{L}_a^p)_{i,i} = 1 - r_i$, and solve the resulting quadratic equation for a :

$$a_i^* \in \frac{-(r_i^{(2)} - \frac{1}{2\mu}) \pm \sqrt{(r_i^{(2)} - \frac{1}{2\mu})^2 - 4\tilde{r}_i^{(1)}\tilde{r}_i^{(3)}}}{2\tilde{r}_i^{(1)}}. \quad (19)$$

We select larger of the two possible values in range $[a^l, a^u]$ as a_i^* . Finally, we compute $a^* = \min_i a_i^*$.

3.4. ADMM Optimization Algorithm

We solve (13) via an ADMM framework [16]. We introduce auxiliary variable $\mathbf{z} = \mathbf{Cx}$, so that (13) can be written as

$$\begin{aligned} & \min_{\mathbf{x}, \mathbf{z}} \|\mathbf{y} - \mathbf{x}\|_2^2 + \mu \|\mathbf{z}\|_1 - \mu \mathbf{x}^\top \mathbf{L}_a^p(\mathbf{x}') \mathbf{x} \\ & \text{s.t. } \mathbf{z} = \mathbf{Cx}. \end{aligned} \quad (20)$$

We write the optimization into an unconstrained form via the augmented Lagrangian method [23]:

$$\begin{aligned} & \min_{\mathbf{x}, \mathbf{z}} \|\mathbf{y} - \mathbf{x}\|_2^2 + \mu \|\mathbf{z}\|_1 - \mu \mathbf{x}^\top \mathbf{L}_a^p(\mathbf{x}') \mathbf{x} \\ & + \xi^\top (\mathbf{z} - \mathbf{Cx}) + \frac{\rho}{2} \|\mathbf{z} - \mathbf{Cx}\|_2^2 \end{aligned} \quad (21)$$

where $\xi \in \mathbb{R}^M$ is a Lagrange multiplier vector, and $\rho \in \mathbb{R}^+$ is an ADMM parameter.

To solve (21), we minimize \mathbf{x} and \mathbf{z} alternately while holding the other variable fixed, until solution convergence. For notation simplicity, we write $\mathbf{L}_a^p = \mathbf{L}_a^p(\mathbf{x}')$ in the sequel.

3.4.1. Optimizing \mathbf{x}^{t+1}

Given fixed \mathbf{z}^t and ξ^t , optimizing \mathbf{x} in (21) becomes

$$\min_{\mathbf{x}} \|\mathbf{y} - \mathbf{x}\|_2^2 - \mu \mathbf{x}^\top \mathbf{L}_a^p \mathbf{x} + (\xi^t)^\top (\mathbf{z}^t - \mathbf{Cx}) + \frac{\rho}{2} \|\mathbf{z}^t - \mathbf{Cx}\|_2^2 \quad (22)$$

which is convex and quadratic. Thus, the optimal \mathbf{x}^{t+1} can be obtained by solving a linear system:

$$(2\mathbf{I} - 2\mu \mathbf{L}_a^p + \rho \mathbf{C}^\top \mathbf{C}) \mathbf{x}^{t+1} = 2\mathbf{y} + \rho \mathbf{C}^\top \mathbf{z}^t + \mathbf{C}^\top \xi^t. \quad (23)$$

Given that the coefficient matrix on the left-hand side is sparse, symmetric and PD, \mathbf{x}^{t+1} can be obtained via *conjugate gradient* (CG) [24] in linear time.

3.4.2. Optimizing \mathbf{z}^{t+1}

Given fixed \mathbf{x}^{t+1} and ξ^t , optimizing \mathbf{z} in (21) becomes

$$\min_{\mathbf{z}} \mu \|\mathbf{z}\|_1 + (\xi^t)^\top (\mathbf{z} - \mathbf{Cx}^{t+1}) + \frac{\rho}{2} \|\mathbf{z} - \mathbf{Cx}^{t+1}\|_2^2. \quad (24)$$

(24) is a sum of a convex smooth function $f(\mathbf{z}) = (\xi^t)^\top (\mathbf{z} - \mathbf{Cx}^{t+1}) + \frac{\rho}{2} \|\mathbf{z} - \mathbf{Cx}^{t+1}\|_2^2$ and convex non-smooth function $g(\mathbf{z}) = \mu \|\mathbf{z}\|_1$. We can thus solve (24) via *proximal gradient descent* (PGD) [16]. Specifically, for each *inner* iteration τ , we compute solution $\mathbf{z}^{\tau+1}$ from previous solution \mathbf{z}^τ as

$$\mathbf{z}^{\tau+1} = \text{prox}_{\lambda g}(\mathbf{z}^\tau - \gamma \nabla f(\mathbf{z}^\tau)) \quad (25)$$

where $\gamma > 0$ is a step size. The gradient $\nabla f(\mathbf{z})$ of $f(\mathbf{z})$ is

$$\nabla f(\mathbf{z}) = \xi^t + \rho(\mathbf{z} - \mathbf{Cx}^{t+1}), \quad (26)$$

and the proximal mapping for $g(\mathbf{z})$ is

$$\text{prox}_{\lambda g}(\mathbf{z}) = \min_{\mathbf{u}} \mu \|\mathbf{u}\|_1 + \frac{1}{2\lambda} \|\mathbf{u} - \mathbf{z}\|_2^2 \quad (27)$$

where $\lambda > 0$ is a proximal mapping parameter. It is known that the solution to (27) is a term-by-term soft-thresholding operation [16]:

$$\text{prox}_{\lambda g}(z_i) = \text{sign}(z_i) \cdot \max(|z_i| - \lambda \mu, 0). \quad (28)$$

3.4.3. Updating ξ^{t+1}

Given fixed \mathbf{x}^{t+1} and \mathbf{z}^{t+1} , Lagrange multiplier ξ^{t+1} can be updated in the conventional manner in ADMM [16]:

$$\xi^{t+1} = \xi^t + \rho (\mathbf{z}^{t+1} - \mathbf{Cx}^{t+1}). \quad (29)$$

4. ALGORITHM UNROLLING

We next unroll each iteration of our ADMM algorithm into a neural layer to compose a feed-forward network for data-driven parameter learning. In addition, we learn a *similarity graph* \mathcal{G} from data, so that incidence matrix \mathbf{C} specifying a positive graph \mathcal{G} in (13) is properly defined.

4.1. Similarity Graph Learning

We define a positive graph \mathcal{G} with edge weights $w_{i,j}$'s that are exponential functions of *Mahalanobis distance* $d_{i,j}$'s:

$$w_{i,j} = \exp(-d_{i,j}), \quad (30)$$

$$d_{i,j} = (\mathbf{f}_i - \mathbf{f}_j)^\top \mathbf{M} (\mathbf{f}_i - \mathbf{f}_j) \quad (31)$$

where $\mathbf{M} \in \mathbb{R}^{K \times K}$ is a PSD *metric matrix*, and $\mathbf{f}_i \in \mathbb{R}^K$ is a K -dimensional feature vector representing pixel i . We compute \mathbf{f}_i via a shallow CNN from an input embedding $\mathbf{e}_i \in \mathbb{R}^E$ that is an image patch centered at pixel i : $\mathbf{f}_i = \text{CNN}(\mathbf{e}_i)$.

4.2. Unrolled Network Architecture

We unroll our ADMM algorithm into T NC-GTV layers. Fig. 1 shows the unrolled network architecture. Each NC-GTV layer has the same structure and parameters. To learn edge weights from data to define \mathbf{C} and \mathbf{L}_a^p , we employ a shallow CNN to learn feature vectors \mathbf{f}_i per pixel i , and then compute edge weights. Parameters μ , ρ , γ and λ in (22) and (24) are trainable parameters in the unrolled network.

Similarly done in [25], the input to the algorithm is $\mathbf{z}^{(0)} = \mathbf{Cy}$ and $\xi^{(0)} = 0$. After T layers, we obtain the reconstruction signal $\mathbf{x}^{(T)}$. The t -th NC-GTV layer uses the output of previous layer, $\mathbf{z}^{(t-1)}$, $\mathbf{x}^{(t-1)}$ and $\xi^{(t-1)}$ and a set of learned

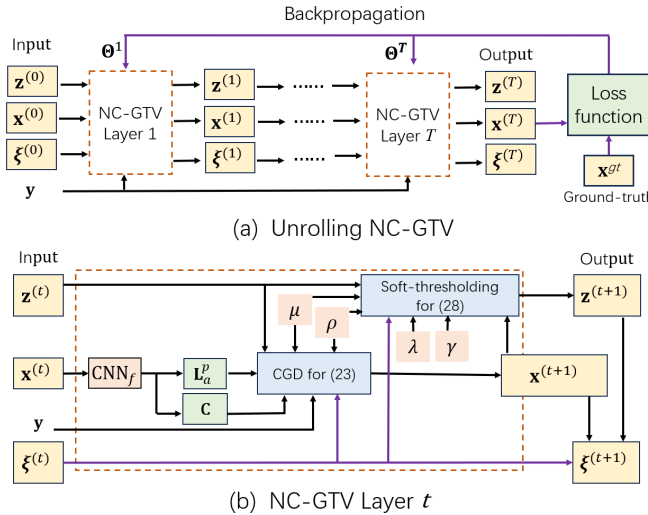


Fig. 1: Overview of the proposed architecture. (a) Unrolled NC-GTV consists of multiple NC-GTV Layers, (b) Block diagram of NC-GTV Layer.

parameters $\Theta^t = \{\rho^{(t)}, \mu^{(t)}, \lambda^{(t)}, \gamma^{(t)}, \theta_f^{(t)}\}$ as input, where $\theta_f^{(t)}$ are the parameters of CNN_f . To train our unrolled network, we evaluate the *mean squared error* (MSE) between the recovered image $\mathbf{x}^{(T)}$ and the ground-truth image \mathbf{x}^{gt} for K training patches to update parameters $\{\Theta^1, \dots, \Theta^T\}$.

5. EXPERIMENTS

5.1. Experimental Setup

We set the number of NC-GTV layers to $T = 2$. CNN_f consists of 4 convolution layers. The first layer has 3 input channels and 32 output channels, while the last layer has 32 and 3. Except for the last layer, we used $\text{ReLU}(\cdot)$ after every convolutional layer. As done in [25], we evaluated our model on the RENOIR dataset and added Gaussian noise to the clean images for experiments. Images were divided into patches of size 36×36 . We trained our model for 200 epochs in each experiment using *stochastic gradient descent* (SGD). The batch size and learning rate were set to 10 and 1×10^{-4} . Our model was implemented in PyTorch and trained on an Nvidia L40 GPU. We compared our model with representative image denoising schemes: model-based CBM3D [17], and DL-based CDnCNN [5], DGLR [26] and DGTB [25]. We evaluated the performance using peak signal-to-noise ratio (PSNR) and structural similarity index measure (SSIM) as metrics.

5.2. Experimental Results

We first trained and tested on additive white Gaussian noise (AWGN) with $\sigma = 30$. Results are shown in Table 1. We observe that learning-based methods generally outperformed model-based CBM3D. Compared to CDnCNN, our model

achieved comparable performance, while using only 18% of network parameters. Our method performed better than previous graph-based schemes DGTB and DGLR.

To demonstrate robustness against noise variance mismatch, we trained all models on AWGN with $\sigma = 30$ and tested them with $\sigma = 50$. As shown in Table 1, NC-GTV achieved the highest PSNR and SSIM. Fig. 2 shows example images of various models.

Table 1: Number of trainable parameters, average PSNR and SSIM in AWGN denoising and noise variance mismatch.

Method	#Parameters	$\sigma_{\text{train}} = 30$		$\sigma_{\text{train}} = 30$	
		$\sigma_{\text{test}} = 30$	$\sigma_{\text{test}} = 50$	$\sigma_{\text{test}} = 30$	$\sigma_{\text{test}} = 50$
CBM3D	N/A	29.11	0.766	N/A	N/A
CDnCNN	0.56M	29.61	0.769	23.88	0.538
DeepGLR	0.93M	29.43	0.746	24.09	0.538
DeepGTV	0.21M	29.36	0.772	24.91	0.572
NC-GTV	0.10M	29.60	0.770	25.43	0.593



Fig. 2: Image examples under a noise variance mismatch scenario: Training on $\sigma = 30$ and testing on $\sigma = 50$.

6. CONCLUSION

Instead of convex total variation (TV) regularization term that underestimates signal discontinuities, we propose non-convex graph total variation (NC-GTV): combine a non-convex regularization term defined by a graph variant of the Huber function with an ℓ_2 -norm fidelity term to compose an overall convex objective, thus mitigating extraneous local minima. We show that our graph Huber function can be understood as a Moreau envelope. We design an iterative optimization algorithm based on alternating direction method of multipliers (ADMM), and unroll it into a lightweight feed-forward network for data-driven parameter learning. Experimental results show that our model has comparable image denoising performance as representative deep learning models, while using a fraction of network parameters.

7. REFERENCES

- [1] P. Milanfar, “A tour of modern image filtering: New insights and methods, both practical and theoretical,” *IEEE Signal Processing Magazine*, vol. 30, no. 1, pp. 106–128, 2013.
- [2] Y. Bai, G. Cheung, X. Liu, and W. Gao, “Graph-based blind image deblurring from a single photograph,” *IEEE Transactions on Image Processing*, vol. 28, no.3, pp. 1404–1418, 2019.
- [3] S. H. Chan, X. Wang, and O. A. Elgendy, “Plug-and-play ADMM for image restoration: Fixed-point convergence and applications,” *IEEE Transactions on Computational Imaging*, vol. 3, no. 1, pp. 84–98, 2017.
- [4] Stanley H. Chan, “Tutorial on diffusion models for imaging and vision,” arXiv preprint arXiv:2403.18103, March 2024, Last revised January 2025.
- [5] K. Zhang, W. Zuo, Y. Chen, D. Meng, and L. Zhang, “Beyond a Gaussian denoiser: Residual learning of deep CNN for image denoising,” *IEEE Transactions on Image Processing*, vol. 26, no. 7, pp. 3142–3155, 2017.
- [6] V. Monga, Y. Li, and Y. C. Eldar, “Algorithm unrolling: Interpretable, efficient deep learning for signal and image processing,” *IEEE Signal Processing Magazine*, vol. 38, no. 2, pp. 18–44, 2021.
- [7] A. Ortega, P. Frossard, J. Kovacevic, J. M. F. Moura, and P. Vandergheynst, “Graph signal processing: Overview, challenges, and applications,” in *Proceedings of the IEEE*, May 2018, vol. 106, no.5, pp. 808–828.
- [8] G. Cheung, E. Magli, Y. Tanaka, and M. Ng, “Graph spectral image processing,” in *Proceedings of the IEEE*, 2018, vol. 106, no.5, pp. 907–930.
- [9] D. Strong and T. Chan, “Edge-preserving and scale-dependent properties of total variation regularization,” *Inverse Problems*, vol. 19, no. 6, pp. S165, nov 2003.
- [10] I. Selesnick, A. Lanza, S. Morigi, and F. Sgallari, “Non-convex total variation regularization for convex denoising of signals,” *Journal of Mathematical Imaging and Vision*, vol. 62, no. 6, pp. 825–841, Jul 2020.
- [11] I. Selesnick, A. Parekh, and İ. Bayram, “Convex 1-D total variation denoising with non-convex regularization,” *IEEE Signal Processing Letters*, vol. 22, no. 2, pp. 141–144, 2015.
- [12] Alessandro Lanza, Serena Morigi, Ivan W. Selesnick, and Fiorella Sgallari, “Sparsity-inducing nonconvex nonseparable regularization for convex image processing,” *SIAM Journal on Imaging Sciences*, vol. 12, no. 2, pp. 1099–1134, 2019.
- [13] P. J. Huber, “Robust estimation of a location parameter,” *Ann. Math. Statist.*, vol. 35, no. 1, pp. 73–101, 1964.
- [14] H. B. Heinz and P. L. Combettes, *Convex Analysis and Monotone Operator Theory in Hilbert Spaces*, Springer, 2017.
- [15] R. S. Varga, *Gershgorin and his circles*, Springer, 2004.
- [16] N. Parikh and S. Boyd, “Proximal algorithms,” in *Foundations and Trends in Optimization*, 2013, vol. 1, no.3, pp. 123–231.
- [17] K. Dabov, A. Foi, V. Katkovnik, and K. Egiazarian, “Image denoising by sparse 3-D transform-domain collaborative filtering,” *IEEE Transactions on Image Processing*, vol. 16, no. 8, pp. 2080–2095, 2007.
- [18] J. Pang and G. Cheung, “Graph Laplacian regularization for inverse imaging: Analysis in the continuous domain,” in *IEEE Transactions on Image Processing*, April 2017, vol. 26, no.4, pp. 1770–1785.
- [19] X. Liu, G. Cheung, X. Wu, and D. Zhao, “Random walk graph Laplacian based smoothness prior for soft decoding of JPEG images,” *IEEE Transactions on Image Processing*, vol. 26, no.2, pp. 509–524, February 2017.
- [20] Abderrahim Elmoataz, Olivier Lezoray, and SÉbastien Bougleux, “Nonlocal discrete regularization on weighted graphs: A framework for image and manifold processing,” *IEEE Transactions on Image Processing*, vol. 17, no. 7, pp. 1047–1060, 2008.
- [21] Camille Couuplie, Leo Grady, Laurent Najman, Jean-Christophe Pesquet, and Hugues Talbot, “Dual constrained TV-based regularization on graphs,” *SIAM Journal on Imaging Sciences*, vol. 6, no. 3, pp. 1246–1273, 2013.
- [22] T. H. Cormen, C. E. Leiserson, and R. L. Rivest, *Introduction to Algorithms*, McGraw Hill, 1986.
- [23] S. Boyd and L. Vandenberghe, *Convex Optimization*, Cambridge, 2004.
- [24] J. R Shewchuk, “An introduction to the conjugate gradient method without the agonizing pain,” Tech. Rep., USA, 1994.
- [25] Huy Vu, Gene Cheung, and Yonina C. Eldar, “Unrolling of deep graph total variation for image denoising,” in *ICASSP 2021 - 2021 IEEE International Conference on Acoustics, Speech and Signal Processing (ICASSP)*, 2021, pp. 2050–2054.
- [26] Jin Zeng, Jiahao Pang, Wenxiu Sun, and Gene Cheung, “Deep graph Laplacian regularization for robust denoising of real images,” in *2019 IEEE/CVF Conference on Computer Vision and Pattern Recognition Workshops (CVPRW)*, 2019, pp. 1759–1768.